

Stable Hydrogen burning limits in rapidly rotating very low mass objects

SHASWATA CHOWDHURY,¹ PRITAM BANERJEE,¹ DEBOJYOTI GARAIN,¹ AND TAPOBRATA SARKAR¹

¹*Department of Physics, Indian Institute of Technology, Kanpur 208016, India*

ABSTRACT

We present novel effects of uniform rapid stellar rotation on the minimum mass of stable hydrogen burning in very low mass stars, using an analytic model, and relaxing the assumption of spherical symmetry. We obtain an analytic formula for the minimum mass of hydrogen burning as a function of the angular speed of stellar rotation. Further, we show the existence of a maximum mass of stable hydrogen burning in such stars, which is purely an artefact of rapid rotation. The existence of this extremum in mass results in a minimum admissible value of the stellar rotation period ~ 22 min, below which a very low mass object does not reach the main sequence, within the ambits of our model. For a given angular speed, we predict a mass range beyond which such an object will not evolve into a main sequence star.

1. INTRODUCTION

Brown dwarfs (BDs), which were theoretically predicted by Kumar (1963), and Hayashi and Nakano (1963), are substellar objects whose masses range between thirteen times that of Jupiter ($\sim 10^{-2}M_{\odot}$) and stars at the bottom of the main sequence ($\sim 10^{-1}M_{\odot}$). During their lifetimes, these “failed stars” do not attain sustained nuclear fusion of Hydrogen into Helium, as their masses are less than a certain minimum value, dubbed as the minimum mass of hydrogen burning (M_{mmhb}) or sometimes as the minimum main sequence mass. Burrows and Liebert (1993) review the works in the area from the mid 60’s to the early 90’s (see also D’Antona and Mazzitelli (1985), Burrows, Hubbard and Lunine (1989)), and provide analytical models of BDs and very low mass (VLM) stars, although their observational aspects were still in the nascent stages at that time, given that BDs are particularly difficult to detect, due to their typically low luminosities. Later, Rebolo, Zapatero-Osorio and Martin (1995) announced the first observation of a brown dwarf in the Pleiades cluster, and this was closely followed by the similar discovery of Nakajima et. al. (1995). The plethora of activities that followed immediately thereafter, are well documented in the review articles by Chabrier and Baraffe (2000), Basri (2000), Burrows et. al. (2001), and the textbook by Rebolo and Zapatero-Osorio (2000) (see also D’Antona and Mazzitelli (1997), Burrows et. al. (1997), Chabrier and Baraffe (1997)). The research carried out in the area in the next decade is outlined in the more recent textbook by Joergens (2014) (see also Allard, Homeier, and Fryetag (2012), Chabrier et. al. (2014), Marley and Robinson (2015)).

What distinguishes BDs from VLM main sequence stars is the M_{mmhb} , with the currently accepted value of $\sim 0.08M_{\odot}$, assuming a static scenario (the recent review of Auddy, Basu and Valluri (2016) quotes the range $0.064 - 0.087M_{\odot}$, based on some modifications of earlier analytical models). However, it is by now well known that various factors may affect the M_{mmhb} , one example being accretion in binary systems (Salpeter (1992)). In this context, we show here that the M_{mmhb} can also be enhanced from its accepted value, via stellar rotation (the physics of rotating stars are described in sufficient details in the older literature, e.g. Kippenhahn and Thomas (1970) and in the recent monographs by Tassoul (2000) and Maeder (2009)). Indeed, more than five decades ago, Kippenhahn (1970) showed a possible increase in the M_{mmhb} due to rotational effects. The basic physics may seem simple. Namely, that with centrifugal forces effectively reducing gravity inside a stellar object, a rotating star can maintain hydrostatic equilibrium at lower core densities and temperatures, thus requiring more mass to achieve thermal stability than its non-rotating cousin. Here one has to keep in mind that in rotating stellar objects, all stellar parameters like the

density, temperature etc., depend on the angular speed of rotation Ω , and that there are several competing effects involving the degeneracy as well. One of the results in this paper is an analytic formula of M_{mmhb} as a function of Ω .

In particular, we consider rapid rotation, where the approximation of spherical symmetry needs to be abandoned. By rapid, we mean a rotation period much smaller than that of Jupiter, which has a period of ~ 10 h. Such rapid rotations in cool dwarfs have been abundantly reported in the recent past. [Clarke et. al. \(2008\)](#) presented photometric observations of a T6 dwarf with a rotation period of 1.41 h. [Metchev, Heinze and Apai \(2015\)](#) presented data on a T7 dwarf with a rotation period of 1.55 h. The analysis of [Route and Wolszczan \(2016\)](#) obtains a dramatically smaller period of ~ 17 min for a T6 dwarf, although the authors point out that this might be a subharmonic of a longer period. Followup observations of the same object by [Williams, Gizis and Berger \(2017\)](#) however indicated that this period might in fact be closer to 1.93 h, although these authors also mention the need for more data to confirm this. The most recent analysis appears in [Tannock et. al. \(2021\)](#), who reported on the observation of photometric periods ranging from 1.08 to 1.23 h. Clearly then, the latest available data on the rapidly rotating brown dwarfs point to the smallest period of 1.08 h, and [Tannock et. al. \(2021\)](#) claim that these are “unlikely” to rotate much faster, given the clustering of the BDs having the smallest rotation periods.

With this status of observational signatures, the question we ask here is, if there are any constraints on rotations of VLM objects set by theory. This is important and interesting for several reasons. First, it is not difficult to imagine that this provides a hitherto unknown dependence of M_{mmhb} with the (rapid) rotational speed Ω , and as we show in sequel, provides quantitative evidence for over-massive BDs, i.e., BDs with mass greater than M_{mmhb} of the non-rotating case. Second, for a given Ω , we obtain a transition mass range $M_{\text{mmhb}}(\Omega) \leq M \leq M_{\text{max}}(\Omega)$ (with $M_{\text{max}}(\Omega)$ being a maximal mass) for stellar objects to evolve into main sequence stars. Finally, we obtain an upper limit of the angular speed $\Omega_{\text{max}} = 0.0047\text{s}^{-1}$, beyond which VLM objects do not evolve into main sequence stars. Importantly, this is not the well known break up angular speed of a star which defines the limit for its disruption in Newtonian gravity via centrifugal forces. The latter is given in a standard fashion for a star of mass M and radius R by $(GM)^{1/2}/R^{3/2}$, where G is the gravitational constant and one assumes spherical symmetry. This formula is true irrespective of the stellar structure equations. To wit, a theoretically infinite number of (M, R) tuples exist for which the Newtonian formula predicts a same break up angular speed. The numerical value quoted above is on the other hand unique, and follows when we self-consistently solve the stellar structure equations in the presence of rapid rotations.

This last statement needs further clarifications. Indeed, as we have already said, the Newtonian formula for the angular speed of disruption is only a quantification of mechanical equilibrium of the stellar object, and does not incorporate aspects of its thermal equilibrium. Specifically, given a limiting angular speed at which a stellar object of a given mass is disrupted, this formula gives an expression for its radius, which one can, to a crude approximation take as the volume equivalent radius of the object. It is however insensitive to the density distribution and degeneracy effects inside the stellar matter. Even if one assumes some form of these latter quantities, the Poisson’s equation, which will result in the gravitational potential at the surface of the object, will be difficult to solve as one does not have well defined boundary conditions there. What we do on the other hand is to perform a self-consistent analysis in which mechanical equilibrium and thermal equilibrium are incorporated simultaneously.

To motivate the need for such analysis, consider, for example, the ratio of the hydrogen burning luminosity of the VLM object to its surface luminosity. Physicality demands that this ratio is less than or equal to unity. In a non-rotating scenario, if this ratio becomes slightly greater than one, then the star will expand, in order to reduce the core temperature, thus achieving balance between internal nuclear energy production and surface energy emission. If the star is rapidly rotating with a given angular speed however, there can be a situation in which further reduction of core density due to internal readjustments, leads to non-existence of model solutions under the assumption of uniform rotation. Clearly then, a consistent numerical analysis taking into account mechanical equilibrium under rapid rotation, in conjunction with the thermal equilibrium conditions, is required.

Here, we adopt the analytical polytropic model of [Burrows and Liebert \(1993\)](#), with some parameters chosen according to Model D, of [Chabrier et. al. \(1992\)](#) (the fourth row of Table 1 of that paper), via a numerical scheme to accommodate rapid rotation (in the non-rotating case, this scenario has been used in [Auddy, Basu and Valluri \(2016\)](#), [Forbes and Loeb \(2019\)](#), [Benito and Wojnar \(2021\)](#)). Indeed, rotating polytropes have been studied for almost a century, starting with [Jeans \(1928\)](#), [Chandrasekhar \(1933\)](#), and later by [Roberts \(1963a\)](#), [Roberts \(1963b\)](#), [Hurley and Roberts \(1964\)](#), [James \(1964\)](#), [Stoeckly \(1965\)](#), etc. The novelty of our work is the implementation of the physics of VLM stars and brown dwarfs in a rapidly rotating scenario. In addition to the results mentioned above, we are also able to provide an analytical formula for the luminosity of a VLM object when it reaches the main sequence, as a

function of its mass and angular speed, within the ambits of this model. These are the main results of this paper. We should mention that we are in effect considering a toy analytical model of VLM objects, where, apart from assuming a polytropic equation of state (EOS), atmospheric corrections are ignored. Modelling the atmospheres of VLM stars and BDs is indeed an active area of current research, see e.g. [Marley and Robinson \(2015\)](#). Incorporating such models along with rapid rotations of VLM objects is indeed a formidable challenge. Our simplified treatment on the other hand brings out several novel physical features of rapidly rotating VLM objects.

The organisation of this paper is as follows. In the next section 2, we recall the basic features of non-rotating VLM objects, and set up the analytical model. This is then used in section 3 to include rotation, and we present our main results in the subsequent section 4. The paper ends with a summary in section 5.

2. NON-ROTATING VLM OBJECTS

The basic assumptions that we use here are as follows. Firstly, the VLM object is assumed to be fully convective, containing helium and partially ionised hydrogen mixture, with partially degenerate electrons in the interior, and helium and molecular hydrogen mixture at the photosphere. The pressure, which arises due to both thermal effects (ions) and degeneracy (electrons) is considered to be non-relativistic. Importantly, these last two assumptions imply that we can safely use a polytropic EOS (polytropic approximations are discussed in the textbook of [Chandrasekhar \(1939\)](#)). For more discussions on the applicability of this approximation to VLM objects, see [Rappaport and Joss \(1984\)](#), [Nelson, Rappaport and Joss \(1986\)](#)). Further, it is assumed that the core temperature in VLM objects is not sufficient to produce He^4 . Hence the truncated $p - p$ chain thermonuclear reactions takes place in the stellar interior. Note that the original model of [Burrows and Liebert \(1993\)](#) model assumes spherical symmetry, which we will relax when we consider rapid stellar rotation.

To set the stage, and to develop the notations used in the rest of this paper, we will now recall some known facts in the evolution of VLM objects. After its formation, during the initial stages, a VLM object keeps contracting owing to its self gravity. In the process, it keeps radiating energy from its surface, which is referred to as surface luminosity L_S . Now, L_S keeps decreasing as the object contracts with time. The contraction, however, initially leads to an increase in its core temperature and density. It is known that rates of thermonuclear reactions are dependent on both of these. Hence, at some stage, if the attained core temperature and density are sufficient, then thermonuclear reactions start taking place. The energy generated within the object due to this is referred to as hydrogen burning luminosity L_{HB} . With further contraction of the object, L_{HB} starts increasing. A stellar object is said to undergo stable/sustained hydrogen burning if the amount of energy liberated from surface is balanced by that produced from thermonuclear reactions within the star i.e., $L_S = L_{HB}$. Hence, at some point during the object's contracting phase, if stable hydrogen burning is attained, then further contraction ceases and the object is said to become a main sequence star (MSS). However, if considerable amount of degeneracy sets in before the object attains stability, a part of the thermal energy of the object is used up in accommodating a large number of degenerate electrons in a smaller volume. This forbids the core temperature from rising further. The core temperature thus starts falling with further contraction. This eventually leads to a decrease in the L_{HB} too, and hence the object does not stabilise thermally. The object is then said to become a BD.

Now, if the initial mass of the object, after formation, happens to be greater than a certain minimum value, then the object eventually stabilises before the onset of considerable electron degeneracy. It is commonly believed that this minimum value, the M_{mmhb} (in the non-rotating case), sets the boundary between a MSS and a BD. Recently, however, [Forbes and Loeb \(2019\)](#) have shown that theoretically over-massive BDs (mass $\gtrsim M_{mmhb}$) are possible, via accretion effects. According to their analysis, M_{mmhb} should no longer demarcate between MSS and BD. However, it is still the minimum main sequence mass.

The continuous contraction of a VLM object, after its formation, leads to increase in its degeneracy. Hence one simulates the time-evolution of an object of a given mass, by varying the degeneracy parameter (called η in sequel). For an object with a given mass, we compute L_{HB} and L_S at every instant of its contracting phase (i.e., lower η value to higher ones). In the process, for every η , we get the value of the ratio of the two luminosities, $L_{ratio} = \frac{L_{HB}}{L_S}$. We then plot L_{ratio} vs η for the given mass. From the above discussions, we see that L_{ratio} first increases, and then starts descending after attaining a maxima. If the maximum value is less than unity, then it indicates that the object can never reach the stable hydrogen burning condition $L_{HB} = L_S$. Hence, we repeat the above numerical procedure for a mass higher than the one previously chosen and repeat the numerical procedure, till the maxima of the plot attains unity. This mass is then the M_{mmhb} . At the point where an object of a given mass attains stable hydrogen burning

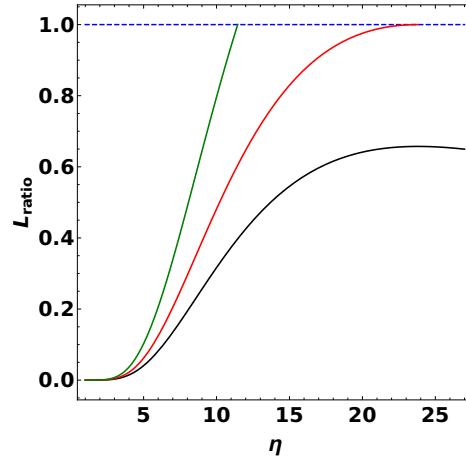


Figure 1. L_{ratio} vs η for non-rotating VLM objects : The red curve corresponds to $M_{\text{mmhb}}(0.081M_{\odot})$, the green one for mass $= 0.085M_{\odot}$ and the black one for $0.078M_{\odot}$.

(i.e. $L_{\text{ratio}} = 1$), it has evolved into a MSS. Thus, from that point onwards one needs to consider a MSS model to further track the evolutionary process. The discussion above is illustrated in Fig. 1, from which one can see that objects having masses greater than M_{mmhb} attains stability (i.e. $L_{\text{ratio}} = 1$) at lower η values.

3. EFFECTS OF ROTATION IN THE VLM OBJECTS' EVOLUTIONARY PROCESS

We first consider the VLM object to be centered at the origin of a Cartesian coordinate system $\{x^1, x^2, x^3\}$. Now we consider uniform rotation of the object along the x^2 -axis. Owing to centrifugal forces, the object bulges near the equatorial plane (i.e. $x^2 = 0$ plane), deforming it into an oblate spheroid. Hence, an object under rapid rotation loses spherical symmetry. The essential features of the analytic model, chosen for studying effects of rapid rotation, are the same as that of [Burrows and Liebert \(1993\)](#), excepting for the assumption of spherical symmetry there, which will lead to crucial modifications as we discuss below.

3.1. The stellar equations and numerical recipe

We begin with the polytropic equation of state, the Poisson's equation, and the Euler equation corresponding to momentum conservation. The polytropic equation reads

$$P = \kappa \rho^{(1+\frac{1}{n})} , \quad (1)$$

where P is the pressure, κ is the polytropic constant and n the polytropic index, which is to be taken as 1.5, as appropriate for VLM objects. The Poisson's equation reads

$$\nabla^2 \phi = 4\pi G \rho , \quad (2)$$

where ρ is the density and ϕ is the gravitational potential. Finally, the Euler equation corresponding to momentum conservation is

$$\rho \frac{\partial v^i}{\partial t} + \rho v^j \frac{\partial v^i}{\partial x^j} = -\frac{\partial P}{\partial x^i} - \rho \frac{\partial \phi}{\partial x^i} , \quad (3)$$

where t is the temporal coordinate and $v^i = \Omega\{x^3, 0, -x^1\}$ is the velocity field of the object, with Ω being its uniform angular speed.

We get the deformed equilibrium configuration of the rotating object of a fixed mass M , by numerically solving Eqs. (2) and (3), for a given κ . Initially we solve the Lane-Emden equation to obtain the spherically symmetric density profile, which is then used in Eq. (2), to obtain the gravitational potential ϕ . Then using this ϕ in Eq. (3), we obtain the updated density profile ρ . We feed this updated ρ back into Eq. (2), to obtain an updated ϕ , which in turn yields an updated ρ from Eq. (3). This iteration is repeated until a desired convergence is achieved for a given tuple $\{M, \Omega, \kappa\}$. For further details of the numerical procedure, the reader is referred to [Ishii, Shibata and Mino \(2005\)](#), [Banerjee et. al. \(2021\)](#).

From the converged solution, we also obtain the central density ρ_c of the deformed object in equilibrium. Now, the polytropic constant is related to the degeneracy parameter (η) of the object as follows

$$\kappa = \frac{(3\pi^2)^{\frac{2}{3}} \hbar^2}{5m_e m_H^{\frac{5}{3}} \mu_e^{\frac{5}{3}}} \left(1 + \frac{\alpha}{\eta}\right), \quad \eta = \frac{(3\pi^2)^{\frac{2}{3}} \hbar^2}{2m_e m_H^{\frac{2}{3}} \mu_e^{\frac{2}{3}} k_B} \frac{\rho^{\frac{2}{3}}}{T}, \quad (4)$$

where m_e and m_H denote the electron and hydrogen mass respectively, and $\alpha = 5\mu_e/2\mu_1$. Here, μ_e is the number of baryons per electron [$\mu_e = 1.143$] and μ_1 is the mean molecular weight of the helium and the partially ionised hydrogen mixture in the interior [$\mu_1 = 0.996$ for Model D of Chabrier et. al. (1992), see Table 1 of Auddy, Basu and Valluri (2016)].

Also note that in Eq. (4), η is defined to be the ratio of the Fermi energy to $k_B T$, where T is the temperature, k_B being the Boltzmann constant. Thus fixing η inherently determines the corresponding κ . We then compute the central temperature T_c from Eq. (4), using the obtained value of ρ_c for the converged equilibrium configuration of the deformed object. Using these, we numerically calculate the hydrogen burning luminosity of the object,

$$L_{HB} = \int_V \rho \epsilon \, dx^1 \, dx^2 \, dx^3, \quad (5)$$

where ρ and ϵ are functions of the spatial coordinates $\{x^1, x^2, x^3\}$, with ϵ being the energy generation rate per unit mass. The integration is performed numerically over the deformed volume V . For VLM objects, with typical values of the core temperature $T_c \sim 3 \times 10^6$ K and core density $\rho_c \sim 10^3 \text{ gm cm}^{-3}$, we can fit ϵ with a power law in T and ρ following Burrows and Liebert (1993), and obtain

$$\epsilon = \epsilon_c \left(\frac{T}{T_c}\right)^s \left(\frac{\rho}{\rho_c}\right)^{u-1}, \quad \epsilon_c = \epsilon_0 T_c^s \rho_c^{u-1} \text{ ergs } g^{-1} s^{-1} \quad (6)$$

with $s \simeq 6.31$, $u \simeq 2.28$ and $\epsilon_0 = 1.66 \times 10^{-46}$. Next, we compute the luminosity at the photosphere (i.e., surface luminosity) of the deformed object. At any point near the surface, the atmosphere can be locally approximated to be plane parallel, irrespective of rotation. Thus we use the following definition of optical depth ($\tau(z)$) for a planar atmosphere to determine the location of photosphere in a deformed object :

$$\tau(z) = \int_z^\infty \kappa_R \rho \, dz, \quad (7)$$

where z is the local vertical depth of the atmosphere and κ_R is the Rosseland mean opacity, taken here to be $0.01 \text{ cm}^2 \text{ g}^{-1}$, which is an order of magnitude estimate, being roughly a tenth of the free electron opacity (see Burrows and Liebert (1993), Forbes and Loeb (2019)). The photosphere is then defined to be located at z_e for which $\tau(z_e) = 2/3$. The temperature T_e and the density ρ_e at the photosphere are related through

$$\frac{T_e}{K} = \frac{b_1 \times 10^6}{\eta^\nu} \left(\frac{\rho_e}{\text{g/cm}^3}\right)^{0.4} \quad (8)$$

where $b_1 = 2.0$ and $\nu = 1.60$ for Model D of Chabrier et. al. (1992), see again Table 1 of Auddy, Basu and Valluri (2016). Now using Eq. (8) and the ideal gas law, and assuming approximate constancy of the acceleration due to gravity near the surface, we obtain a local expression for the temperature at the photosphere.

$$T_e = \left(\frac{2g\mu_2 m_H}{3\kappa_R k_B}\right)^{\frac{0.4}{1.4}} \left(\frac{b_1 \times 10^6}{\eta^\nu}\right)^{\frac{1}{1.4}}. \quad (9)$$

where μ_2 is the mean molecular weight of the helium and molecular hydrogen mixture at the photosphere [$\mu_2 = 2.285$]. For a deformed object, the relative position of the photosphere with respect to the surface of the object does not remain constant throughout, i.e., it varies from one surface point to another, unlike the case for a spherically symmetric object. This would also be the case with T_e . Now applying Stefan-Boltzmann law, we compute the total surface luminosity as

$$L_S = \oint_S \sigma T_e^4 \, dA \quad (10)$$

where dA is the elemental surface area and σ is the Stefan-Boltzmann constant. The integration is performed over the entire surface of the deformed object. Finally, we compute the L_{ratio} for the given $\{M, \Omega, \eta\}$, which would be of fundamental importance to decide upon the fate of a rotating object's evolution. It should be noted that in the limiting case of $\Omega \rightarrow 0$, we recover the original model due to Burrows and Liebert (1993).

4. RESULTS AND ANALYSIS

We now present the main results obtained from our computational scheme discussed above.

4.1. M_{mmhb} as a function of Ω

Rotation tends to reduce the strength of gravity inside a star. This effectively makes a rotating star, achieve hydrostatic equilibrium at a lower core temperature and density. As a result total nuclear energy production is reduced, so a higher mass is required to achieve thermal stability ($L_{\text{ratio}} = 1$). Hence we find that the M_{mmhb} , in presence of rotation to be larger than non rotating case. In order to find M_{mmhb} corresponding to a given stellar rotation Ω , we carry out a similar algorithm described in section 2, using the numerical prescription mentioned in section 3.1. We perform this numerical procedure for different Ω values, to obtain a fitted formula for M_{mmhb} as a function of Ω . We find,

$$M_{\text{mmhb}}(\Omega) = 0.0814 + 0.2302\Omega + 245.58\Omega^2 + 67646\Omega^3, \quad (11)$$

where Ω is in s^{-1} and the formula gives $M_{\text{mmhb}}(\Omega)$ in units of the solar mass M_{\odot} . From Eq. (11), we find that M_{mmhb} increases monotonically with Ω as depicted by the red curve in Fig. 4, but that for small Ω , the change from the case $\Omega = 0$ is maximally by a few percents. For example, for the smallest observed period of 1.08 h of Tannock et. al. (2021), the increase in M_{mmhb} is by $\sim 1.6\%$. Faster rotations can however significantly change the result. Using the period of 17 min of Route and Wolszczan (2016), the increase in M_{mmhb} is $\sim 33\%$. However, such a small value of the period is ruled out of our analysis, as we momentarily see. We will find that the minimum period of a VLM star can be ~ 22 min, and hence the maximal increase in M_{mmhb} is $\sim 17\%$. Importantly, we have demonstrated that rotation can lead to the existence of over-massive BDs without accretion effects.

As an aside, we note the behavior of M_{mmhb} with Ω for the two extreme models of Chabrier et. al. (1992) - Model A and Model H in Auddy, Basu and Valluri (2016). For Model A we obtain $M_{\text{mmhb}}(\Omega) = 0.0879 + 0.2441\Omega + 220.53\Omega^2 + 60446\Omega^3$, while for Model H we obtain $M_{\text{mmhb}}(\Omega) = 0.0636 + 0.2113\Omega + 445.97\Omega^2 + 117094\Omega^3$. The increase in M_{mmhb} , corresponding to the smallest observed rotation period of 1.08 h of Tannock et. al. (2021), is by $\sim 1.4\%$ for Model A and $\sim 3.1\%$ for Model H. The smaller period of 17 min of Route and Wolszczan (2016) corresponds to an increase in M_{mmhb} by $\sim 27\%$ and $\sim 72\%$ for Model A and Model H respectively. However, such a small value of the rotation period ~ 17 min, falls below the minimum permissible periods corresponding to both Model A and H, and is thus ruled out of our analysis. The minimum permissible period for Model A is ~ 20 min, which corresponds to a maximal increase in M_{mmhb} by $\sim 19\%$. For Model H, the maximal increase in M_{mmhb} is by $\sim 21\%$ corresponding to the minimum permissible period of ~ 28 min.

4.2. Behavior of L_{ratio} vs η plot for non-zero stellar rotation :

The L_{ratio} vs η plot for VLM objects corresponding to a given non-zero rotation Ω is very different from its non-rotating counterpart (compare Fig. 1 with Fig. 2). Here we observe that for a given mass and rotation, the L_{ratio} vs η curve starts from a particular point (let us call it the critical point). The particular values of η and L_{ratio} corresponding to the critical point are referred to as the η_{crit} and critical L_{ratio} respectively, for that particular mass and rotation. As an example, $\eta_{\text{crit}} = 5.18$ and critical $L_{\text{ratio}} = 0.09$ for a VLM object of mass $M = 0.1M_{\odot}$ rotating with angular speed of $\Omega = 0.003s^{-1}$ (the filled black circle where the blue line culminates in Fig. 2). A VLM object of given mass and rotation, cannot achieve hydrostatic equilibrium for η values lower than its corresponding η_{crit} . The reason is as follows. A VLM object cannot sustain a given rotation, unless it possesses a certain minimum central density, dubbed as critical density, ρ_{crit} . We also know that during the contraction phase of a VLM object, its central density ρ_c increases with an increase in degeneracy η . Hence the central density at η_{crit} for any VLM object of a given mass and rotation, denotes the minimum value of central density below which the object cannot sustain the applied rotation (i.e., for central densities corresponding to $\eta \leq \eta_{\text{crit}}$ no model solution exists). As Fig. 2 indicates, for a particular Ω , higher mass VLM objects attain the corresponding critical density at lower η_{crit} values and the corresponding critical L_{ratio} are higher. It is observed from that figure that for a given rotation, higher mass objects reach the main sequence at lower value of η . The mass value for which critical $L_{\text{ratio}} = 1$ will be called as M_{max} for the given Ω . For example $M_{\text{max}} = 0.29 M_{\odot}$ for $\Omega = 0.003s^{-1}$ (See Fig. 2). In Fig. 2, the black dot-dashed line represents the locus of critical points (marked by filled circles) of the curves corresponding to different masses ranging from M_{mmhb} to M_{max} and is a portion of the critical L_{ratio} vs η curve in Fig. 3, which we now explain.

4.3. The Existence of M_{max}

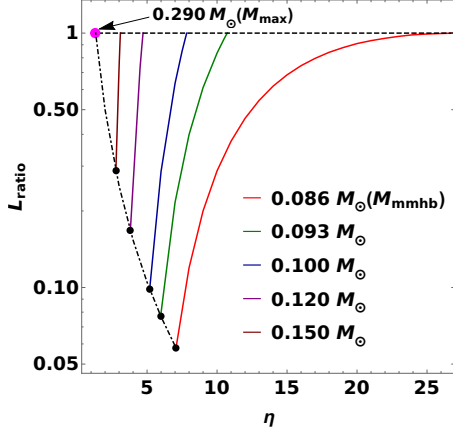


Figure 2. L_{ratio} vs η plot for $\Omega = 0.003s^{-1}$. The red curve corresponds to M_{mmbb} . As explained in the text, it starts from $\eta = \eta_{\text{crit}}$ and non-zero critical L_{ratio} , represented by the corresponding filled black circle. It reaches main sequence when $L_{\text{ratio}} = 1$. For higher masses, η_{crit} is lower and critical L_{ratio} is higher. Higher mass objects reach the main sequence at lower values of η . The mass value for which critical $L_{\text{ratio}} = 1$ (here $0.29 M_{\odot}$), is the M_{max} for this Ω . The black dot-dashed line represents the locus of critical points (marked by filled circles) of the curves corresponding to different masses ranging from M_{mmbb} to M_{max} , for this Ω . M_{max} is marked by the filled magenta circle.

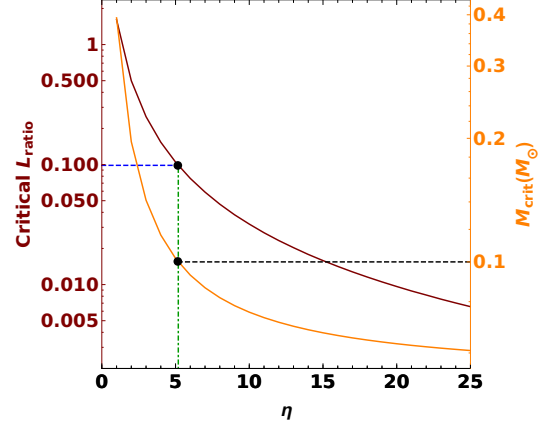


Figure 3. Critical L_{ratio} vs η and M_{crit} vs η plot for $\Omega = 0.003s^{-1}$. The brown curve corresponds to critical L_{ratio} , while the orange one corresponds to M_{crit} . The point on the critical L_{ratio} curve, which corresponds to 0.098, is the top filled black circle. The vertical line from that point intersects the η axis at corresponding η_{crit} (5.18). The point of intersection between the same vertical line and the M_{crit} curve, gives the corresponding M_{crit} ($0.1M_{\odot}$). Each y-axis is color coded to the data.

As we have already indicated, for central densities lesser than ρ_{crit} , no model solution is possible for a VLM object of given mass and angular speed for which we are referring the ρ_{crit} . We call the stellar configuration as a critical configuration when the central density equals ρ_{crit} . For a given Ω , we find the critical configuration for each value of the degeneracy η . For each of these critical stellar configurations, we record the critical density ρ_{crit} and compute the critical value of L_{ratio} as well as the critical mass, which we call M_{crit} . While we find that ρ_{crit} remains constant with η , Fig. 3 indicates that both critical L_{ratio} and M_{crit} falls with increasing degeneracy, as is not difficult to justify physically from the following :

- For a given Ω , we have seen that the critical density remains constant with increase in η . We also know with increase in η , the κ value decreases according to Eq. (4). Hence, with increase in η the central pressure for the corresponding critical configurations keeps decreasing according to the formula for polytropic EOS. We know that reduced central pressure can support lower stellar mass. Hence, for a given Ω , increase in η leads to decrease in M_{crit} .
- For a given Ω , with increase in η value, the central temperature corresponding to the critical configuration keeps decreasing according to Eq. (4), owing to constancy of ρ_{crit} . This leads to reduction in L_{HB} and hence L_{ratio} for the corresponding critical configurations.

The information that one obtains from the plot in Fig. 3 is the particular minimum value of η ($= \eta_{\text{crit}}$) at which a VLM object of given mass M_{crit} , has just the sufficient central density ρ_{crit} , in order to sustain the given rotation Ω . One also obtains the value of the corresponding critical L_{ratio} . From η_{crit} onwards, as the object of that particular mass M_{crit} keeps contracting, the systematic behavior of L_{ratio} vs η follows. At this point one can draw complete correspondence between Fig. 3 and Fig. 2. For example, in Fig. 3, we see a VLM object of mass $0.1M_{\odot}$ attains

the critical density at $\eta_{\text{crit}} = 5.18$ and the corresponding critical $L_{\text{ratio}} = 0.098$. This particular mass object will not possess any model solution for η values less than η_{crit} under the given rotation. Hence, we see from Fig. 2, the L_{ratio} vs η curve for object of mass $0.1M_{\odot}$ starts from the point ($\eta = 5.18$, $L_{\text{ratio}} = 0.098$). From that point onwards, as the given object contracts, the central density keeps increasing along with an increase in degeneracy η . Thus the model solutions for the object will exist under the given rotation for $\eta \geq \eta_{\text{crit}}$, and we get the systematic plot of L_{ratio} vs η for that particular object starting from $\eta = \eta_{\text{crit}}$.

For a given Ω , the critical L_{ratio} value corresponding to η_{crit} of a specified mass object reveals the relative magnitude of hydrogen burning luminosity and surface luminosity, at the initial stage of its evolution, when it has attained sufficient degeneracy to sustain the given rotation. Three situations can arise at this particular critical point. Firstly, if critical $L_{\text{ratio}} < 1.0$, the object will attain stability with further evolution, only if $M \geq M_{\text{mmhb}}(\Omega)$. Secondly, for critical $L_{\text{ratio}} = 1$, the object has already turned into a MSS. We label the corresponding mass as M_{max} for the given Ω . Finally, for critical $L_{\text{ratio}} > 1.0$, the hydrogen burning luminosity exceeds surface luminosity and our VLM object can never stabilize while maintaining the given uniform rotation. We will show this explicitly in a moment. Hence, for a given Ω , the valid range of mass M , for which a VLM object can eventually evolve into a MSS, is $M_{\text{mmhb}} \leq M \leq M_{\text{max}}$. We call this M_{max} as the maximum mass of stable hydrogen burning for this Ω and as is clear from the context, the quantity M_{max} is purely an artefact of rotational effects. We shall refer to this mass range as the transition mass range.

Let us now comment upon the case critical $L_{\text{ratio}} > 1.0$. To understand this, we use the standard stellar energy equation $\dot{\epsilon} - \partial L / \partial M = T dS / dt$, where L denotes the luminosity, M the mass, T the temperature and S is the entropy per unit mass. Integrating this equation, we get after a little bit of algebra,

$$L_S(1 - L_{\text{ratio}}) = \frac{K}{\eta^2} \frac{d\eta}{dt} \int \rho^{5/3} dV, \quad K = 5.25 \times 10^5 \frac{N_A k_B}{\mu_e^{2/3}}, \quad (12)$$

with N_A being Avogadro's number and k_B the Boltzmann's constant. Clearly then, at η_{crit} , if critical $L_{\text{ratio}} > 1$, Eq. (12) dictates that $d\eta/dt < 0$, and in this case, the object will not possess a model solution below the minimum degeneracy η_{crit} for the given Ω .

4.4. M_{max} as a function of Ω

The concept of a critical density is only valid for a rotating stellar object. For a non-rotating stellar object, M_{max} is not defined. This means that any non-rotating object of mass $M \geq M_{\text{mmhb}}$ can in principle evolve to the main sequence. In order to find M_{max} corresponding to a given non-zero stellar rotation Ω , we numerically compute the M_{crit} value corresponding to critical $L_{\text{ratio}} = 1.0$. For example from Fig. 3, one can see that the M_{crit} value corresponding to critical $L_{\text{ratio}} = 1.0$ is $0.29M_{\odot}$, which is the M_{max} for $\Omega = 0.003s^{-1}$. We perform this numerical procedure for different Ω values, to obtain a fitted formula for M_{max} as a function of Ω . We find in units of M_{\odot} ,

$$M_{\text{max}}(\Omega) = -1.2621 + 0.0176\Omega^{-1} - 7.7873 \times 10^{-5}\Omega^{-2} + 1.1648 \times 10^{-7}\Omega^{-3} \quad (13)$$

where Ω is in s^{-1} . From Fig. 4, which depicts this behavior, one can see that with increase in Ω , M_{max} decreases. This can be explained as follows. We already know that for a given Ω , M_{max} corresponds to mass of the particular critical configuration, for which stable hydrogen burning takes place at the critical point. Now, for a higher value of Ω , the corresponding critical configuration maintains hydrostatic equilibrium at higher central density and temperature. As a consequence, total nuclear energy production gets magnified, resulting in critical $L_{\text{ratio}} > 1.0$. So a lower mass is needed to attain thermal stability at the critical point (i.e. critical $L_{\text{ratio}} = 1.0$). As a consequence, M_{max} decreases with increase in Ω .

For Ω values less than $0.003s^{-1}$, the corresponding M_{max} values are larger than $0.3M_{\odot}$ beyond which an object is no longer in fully convective equilibrium. Hence those points are not shown in Fig. 4.

From the behavior of M_{mmhb} and M_{max} with Ω , we see gradual decrease in the transition mass range $[M_{\text{mmhb}}(\Omega), M_{\text{max}}(\Omega)]$, with increase in Ω . There exists a certain $\Omega = 0.0047 s^{-1}$, where the two curves $M_{\text{mmhb}}(\Omega)$ and $M_{\text{max}}(\Omega)$ meet (this is not the one obtained by visual inspection in Fig. 4 where the two quantities are drawn with different scales). Consequently the distinctive transition mass range reduces to a single point at this particular Ω . We shall call this angular speed Ω_{max} . Thus according to our model, for stellar rotations with angular speeds more than $\Omega_{\text{max}} \sim 0.0047 s^{-1}$ (or rotation periods less than ~ 22 min), a VLM object cannot evolve into a MSS.

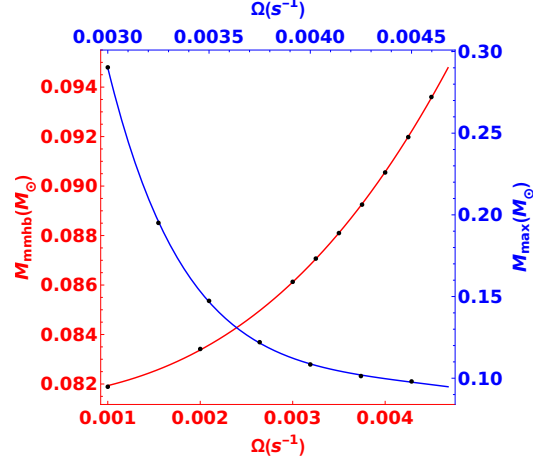


Figure 4. The red curve corresponds to $M_{\text{mmhb}}(\Omega)$, while the blue one corresponds to $M_{\text{max}}(\Omega)$. Each y-axis is color coded to the data.

4.5. Stable Luminosity Formula

Finally, we deduce a formula for the stellar Luminosity (L_{HB} due to H-burning), at the point when object reaches the main sequence, after initial evolution. This is denoted by \tilde{L}_{HB} and is a function of both the stellar mass and the stellar rotation. The lowest order polynomial which best fits our generated data is represented as $\tilde{L}_{HB}(M, \Omega)/L_{\odot} = \sum_{\alpha, \beta} C_{\alpha\beta} (M/M_{\odot})^{\alpha} (\Omega/s^{-1})^{\beta}$, and the coefficients $C_{\alpha\beta}$ are listed in Table 1. Fig. 5 represents the contour plot of

Table 1. List of coefficients $C_{\alpha\beta}$

$\alpha \backslash \beta$	0	1	2	3	4	5	6
0	24.203	1265.4	95238	1.2927×10^6	6.7610×10^6	7.3972×10^9	1.114×10^{11}
1	-1577.2	-70298	-4.1388×10^6	-3.3679×10^7	-8.8127×10^8	-1.0444×10^{11}	—
2	42761	1.5598×10^6	6.6859×10^7	2.8294×10^8	1.0488×10^{10}	—	—
3	-6.1736×10^5	-1.7279×10^7	-4.7498×10^8	-7.9453×10^8	—	—	—
4	5.0065×10^6	9.5552×10^7	1.2490×10^9	—	—	—	—
5	-2.1626×10^7	-2.1102×10^8	—	—	—	—	—
6	3.8887×10^7	—	—	—	—	—	—

\tilde{L}_{HB} . All the objects, having particular masses and rotations (M, Ω) tuples, constituting any given contour, will end up in the main sequence, with the same luminosity. The results from this plot are not to be extrapolated beyond the valid range of transition mass ($M_{\text{mmhb}}(\Omega) \leq M \leq M_{\text{max}}(\Omega)$, where $\Omega \in (0, \Omega_{\text{max}})$), since beyond this range, an object never evolves into a MSS.

It has been observed that our model parameters (corresponding to Model D of Chabrier et. al. (1992)) succeeds in reproducing reasonable estimates of stellar luminosities, characteristic to the VLM objects up to a maximal mass of $\sim 0.1M_{\odot}$. Hence the confidence in our model lies precisely in the region:

$$M_{\text{mmhb}}(\Omega) \leq M \leq M_{\text{max}}(\Omega) , \quad \text{with } M \leq 0.1M_{\odot} , \quad \text{and } 0 \leq \Omega \leq \Omega_{\text{max}} . \quad (14)$$

In Fig. 5, we have shown the \tilde{L}_{HB} contours within the above mentioned region. The blue curve represents $M_{\text{max}}(\Omega)$, while the red one corresponds to $M_{\text{mmhb}}(\Omega)$.

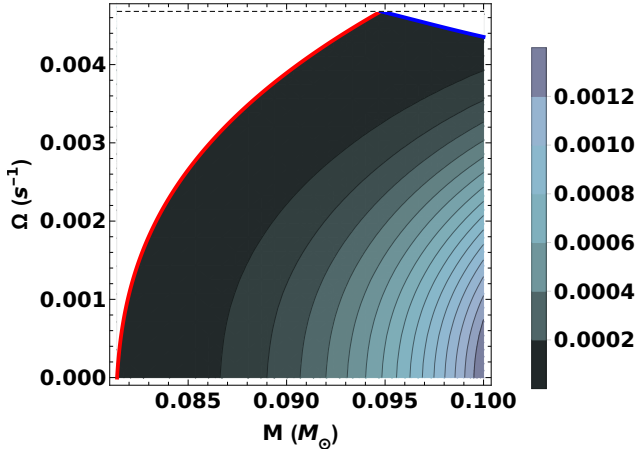


Figure 5. \tilde{L}_{HB} Contours. Any particular contour of \tilde{L}_{HB} specifies all admissible values of mass M and rotation Ω of VLM object, that acquire the same hydrogen burning luminosity when they reach the main sequence. The validity of this contour plot lies in the admissible range of $M_{\text{mmhb}}(\Omega) \leq M \leq M_{\text{max}}(\Omega)$ with maximal M and Ω values of $0.1M_{\odot}$ and $0.0047s^{-1}$. The red curve represents the $M_{\text{mmhb}}(\Omega)$, while the blue curve represents the $M_{\text{max}}(\Omega)$.

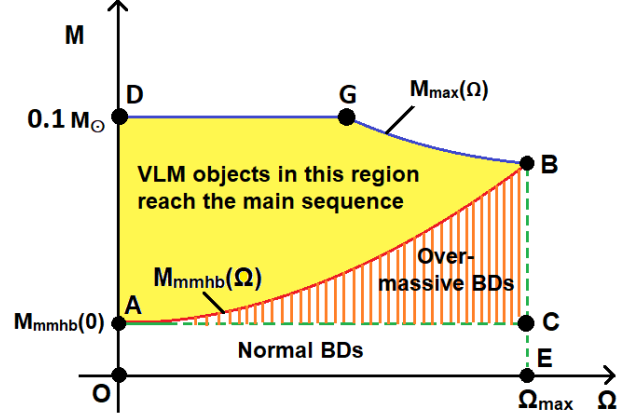


Figure 6. Schematic diagram of the results obtained in this paper. $M_{\text{mmhb}}(0)$ corresponds to $M_{\text{mmhb}}(\Omega = 0)$. See discussion in text.

5. DISCUSSIONS

In this paper, we have used a simplified analytical model to study the effects of rapid rotation on the M_{mmhb} . Our model is inspired by the one due to Burrows and Liebert (1993) to which it reduces to, in the limiting non-rotating case. Following Auddy, Basu and Valluri (2016), we have chosen the values of some of the model parameters from Model D of Chabrier et. al. (1992) in order to obtain reasonable estimates for the physical parameters. There are four main results that we have obtained.

- We have found an analytical formula of the M_{mmhb} as a function of the angular speed Ω .
- For a given Ω , we have obtained the mass range $M_{\text{mmhb}}(\Omega) \leq M \leq M_{\text{max}}(\Omega)$ for VLM objects to evolve into main sequence stars.
- We have obtained an upper bound $\Omega_{\text{max}} = 0.0047s^{-1}$ beyond which a VLM object will not evolve into a MSS.
- As a by-product of our analysis, we obtained the luminosity of a VLM object at the point where it reaches the main sequence, as a function of M and Ω .

A schematic diagram of the main results in the paper is given in Fig. 6. Here, the red curve AB represents $M_{\text{mmhb}}(\Omega)$. The blue curve DG represents the maximal mass of $0.1M_{\odot}$. The blue curve GB represents portion of the $M_{\text{max}}(\Omega)$ up to a maximal mass of $0.1M_{\odot}$. The two curves AB and GB intersect at point B. Point A corresponds to M_{mmhb} value for the non rotating case, labeled as $M_{\text{mmhb}}(0)$ in the figure. The horizontal line AC denotes a constant mass curve corresponding to the M_{mmhb} for the non-rotating case. Also, O corresponds to origin, while E denotes Ω_{max} . Over-massive BDs (in the region ABC), have been shown to exist purely due to uniform stellar rotation. In absence of rotation, BDs lie in the region ACEO, labeled as “Normal BDs.” The VLM objects in the region DGBA can evolve into MSS.

Here, we have used a toy model, with a number of assumptions. First, all the thermodynamic relations have been assumed to remain unaltered in the presence of rotation. This can be justified, as the rotational kinetic energy $I\Omega^2/2$ with I being the moment of inertia of the deformed object computed numerically, can always be shown to be two

orders of magnitude lower than the gravitational potential energy. Second, we have considered the effect of uniform stellar rotation on VLM object's evolution. A more realistic situation with differential and time-varying rotation is left for a future study. Third, in our analysis of stellar evolution under constant uniform rotation, the non-conservation of angular momentum has been inherently assumed. Finally, our model is polytropic, and does not take account of atmospheric corrections and related details.

However, this simplistic toy model has successfully been able to decode the underlying physics of a rapidly rotating VLM object and has revealed several important limits.

6. ACKNOWLEDGMENTS

We thank our anonymous referee for various important comments which helped to improve an initial version of the manuscript. We acknowledge the High Performance Computing (HPC) facility at IIT Kanpur, India, where the numerical analysis was carried out.

REFERENCES

- Allard, F., Homeier, D., and Freytag, B., *Phil. Trans. R. Soc. A* (2012), **370**, 2765.
- Auddy, S., Basu, S., and Valluri, S. R., 2016, *Adv. Astron.*, 2016, 5743272.
- Banerjee, P., Garain, D., Paul, S., et. al., 2021, *Astrophys. J.* **910**, 23.
- Basri, G., 2000, *Ann. Rev. Astron. Astrophys.* **38**, 485.
- Benito, M., and Wojnar, A., *Phys. Rev. D* **103**, no.6, 064032.
- Burrows, A., Hubbard, W. B., and Lunine, J. I., 1989, *Astrophys. J.* **345**, 939.
- Burrows, A., Hubbard, W. B., Lunine, J. I., and Liebert, J., 2001, *Rev. Mod. Phys.* **73**, 719.
- Burrows, A., and Liebert, J., 1993, *Rev. Mod. Phys.* **65**, 301.
- Burrows, A., Marley, M., and Hubbard, W. B., *Astrophys. J.* **491**, 856.
- Chabrier, G., Saumon, D., Hubbard, W., B., Lunine, J. I., 1992, *Astrophys. J.* 391, 817.
- Chabrier, G., and Baraffe, I., 1997, *Astron. Astrophys.* 327, 1039.
- Chabrier, G., and Baraffe, I., 2000, *Ann. Rev. Astron. Astrophys.* **38**, 337.
- Chabrier, G., Johansen, A., Janson, M., Rafikov, R., 2014, in Beuther, Henrik, et al. *Protostars and Planets VI*, University of Arizona Press, 619.
- Chandrasekhar, S., 1933, *MNRAS* **93**, 390.
- Chandrasekhar, S., *An Introduction to the Study of Stellar Structure*, 1939, Univ. of Chicago Press, U.S.A.
- Clarke, F. J., Hodgkin, S. T., Oppenheimer, B. R., et. al., 2008, *MNRAS* **386**, 2009.
- D'Antona, F., and Mazzitelli, I., 1985, *Astrophys. J.* **296**, 502.
- D'Antona, F., and Mazzitelli, I., 1997, *Memorie della Societa Astronomica Italiana* **68**, 807.
- Forbes, J. C., and Loeb, A., 2019, *Astrophys. J.* **871**, 2.
- Hayashi C., and Nakano T., 1963, *Prog. Theor. Phys.* **30**, 460.
- Hurley, M., and Roberts, P. H., 1964, *Astrophys. J.*, **140**, 583.
- Ishii M., Shibata M. and Mino Y., 2005, *Phys. Rev. D*, **71**, 044017.
- James, R., 1964, *Astrophys. J.*, **140**, 552.
- Jeans, J. H., 1928, *Astronomy and Cosmogony*, Cambridge University Press, U.K.
- Joergens, V., Ed., 2014, *50 Years of Brown Dwarfs, From Prediction to Discovery to Forefront Research*, Springer, Heidelberg.
- Kippenhahn, R., 1970, *Astron. Astrophys.* **8**, 50.
- Kippenhahn, R., and Thomas, H. C., 1970, in Slettebak, A., Ed., *Stellar Rotation Proc. IAU Colloquium 1969*, D. Reidel Publishing Company, Dordrecht-Holland.
- Kumar, S. S., 1963, *Astrophys. J.* **137**, 1121.
- Maeder, A., 2009, *Physics, Formation and Evolution of Rotating Stars*, Springer-Verlag, Berlin, Heidelberg.
- Marley, M. S., and Robinson, T. D., *Ann. Rev. Astron. Astrophys.* (2015), **53**, 279.
- Metchev, S. A., Heinze, A., Apai, D., et al. 2015, *Astrophys. J.* **799**, 154.
- Nakajima, T., Oppenheimer, B., Kulkarni, S. et al., 1993, *Nature* **378**, 463.
- Nelson, L. A., Rappaport, S. A., and Joss, P. C., 1986, *Astrophys. J.* **311**, 226.
- Rappaport, S., and Joss, P. C., 1984, *Astrophys. J.* **283**, 232.
- Rebolo, R., and Zapatero-Orsorio, M., R., 2000, *Very Low-Mass Stars and Brown Dwarfs*, Cambridge University Press, Cambridge, United Kingdom.
- Rebolo, R., Zapatero-Orsorio, M., R., and Martin, E., 1995, *Nature* **377**, 129.
- Roberts, P. H., 1963, *Astrophys. J.*, **137**, 1129.

- Roberts, P. H., 1963, *Astrophys. J.*, **138**, 809.
- Route, M., and Wolszczan, A., 2016, *Astrophys. J. Letters* **821** L21.
- Salpeter, E. E., 1992, *Astrophys. J.* **393**, 258.
- Stoeckly, R., 1965, *Astrophys. J.*, **165**, 208.
- Tannock, M. E., Metchev, S., Heinze, A., et. al. (2021) *Astron. J.* **161**, 224.
- Tassoul, J-L., 2000, **Stellar Rotation**, Cambridge University Press, Cambridge, United Kingdom.
- Williams, P. K. G., Gizis, J. E., and Berger, E., *Astrophys. J.* 2017, **834**, 117.